



UNITED NATIONS
UNIVERSITY

GEOHERMAL TRAINING PROGRAMME
Orkustofnun, Grensasvegur 9,
IS-108 Reykjavik, Iceland

Reports 2011
Number 32

PRELIMINARY RESERVOIR ANALYSIS OF MENENGAI GEOTHERMAL FIELD EXPLORATION WELLS

Janet Jelagat Suwai

Geothermal Development Company Ltd. – GDC

P.O. Box 17700 – 20100

Nakuru

KENYA

jsuwai@gdc.co.ke

ABSTRACT

Drilling in Menengai geothermal field started in February 2011 with the aim of harnessing steam for electricity power production. Three exploration wells have been completed and are still undergoing different measurements and tests. Results of 80 days of flow testing indicate that MW-1 produces two-phase fluid with an enthalpy of over 1200 kJ/kg, and a production capacity of more than 6 MWe. Temperature recovery in MW-2 has been interfered with by the upper cold feed zones. MW-2 transmissivity and storativity values are in the range 8.56×10^{-8} - 11.7×10^{-8} m³/Pa·s and 1.48×10^{-7} - 1.58×10^{-7} m/Pa, respectively. Heat-up profiles in MW-3 indicate a cold section between 1200 and 1500 m depth, with a conductive section below 1600 m. Preliminary reserve estimation, using volumetric calculation, indicates with 90% confidence that the electricity production within the Menengai caldera could reach 570 MWe for a production period of 30 years and up to 375 MWe for a period of 50 years.

1. INTRODUCTION

Menengai geothermal field (Figure 1) encompasses the Menengai volcano, the Ol-Rongai volcanoes, Ol-Banita plains and parts of the Solai graben to the northeast. This is the area bound by eastings 157000 and 185000 and northings 9966000 and the Equator (Arc 1960/UTM zone 37S). Regional exploration for geothermal resources in Kenya indicates that the Quaternary volcanic complexes within the Kenya rift valley provide the most promising prospects for geothermal exploration (Dunkley et al., 1993).

A detailed exploration of the geothermal resources in the Menengai area was conducted in 2004 and later with infill work in 2010. Geoscientific investigations comprising geology, geophysics, geochemistry and heat loss measurements were utilized in searching for indicators for the existence of geothermal resources in the area. Findings presented in Lagat et al. (2010) and Mungania (2004) point to the existence of exploitable geothermal resources within the Menengai caldera, Ol-Rongai and Ol-Banita calderas to the northwest of the Menengai caldera. The existence is evidenced by active strong surface manifestations and young lavas, signifying an active heat source. Geophysical analysis indicates a hot magmatic body underlying the caldera structure (Simiyu and Keller, 2001).

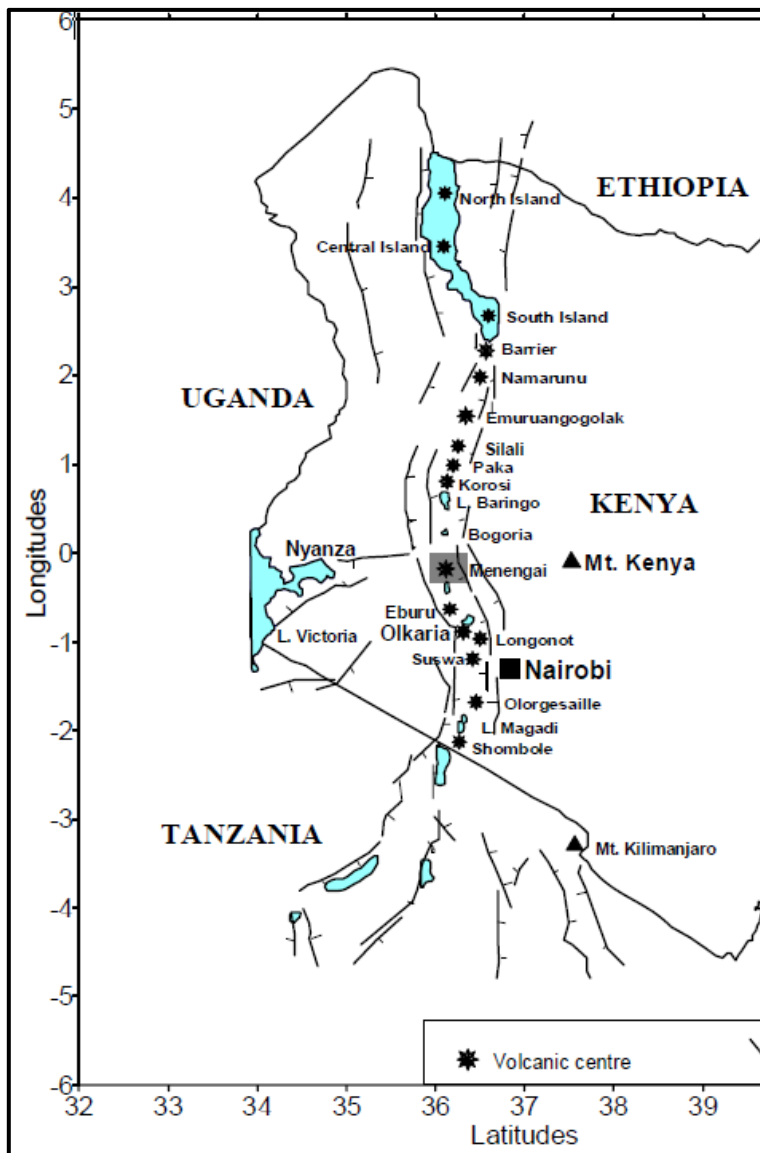


FIGURE 1: Map of Kenya showing location of the Menengai geothermal area and other volcanic systems along the Kenya rift (Wameyo, 2005)

According to models, the hot magmatic body resulted in the development of a geothermal system with an up-flow under the caldera and an outflow to the north (Figure 2). Seismic studies by Simiyu and Keller (1997) indicate clusters of shallow micro-earthquakes under the caldera and relate these to a high-temperature geothermal field associated with shallow magma bodies. A heat loss survey indicates that the prospect loses about 3,536 MWt naturally to the atmosphere with 2440 MWt being the convective component (Mwawongo, 2005).

Reservoir temperatures deduced from gas geothermometry were estimated to be more than 280°C (Lagat et al., 2010). Efforts to harness the untapped geothermal energy led to the siting of exploratory wells MW-1, MW-2, and MW-3 (see Figure 2). It was decided to drill them as normal production wells, so they could serve as both exploratory wells and production wells (or injection wells) once the field has been developed further. This report presents the preliminary findings from well measurements and tests conducted in the first three exploration wells of Menengai geothermal field.

1.1 General geological setting

The East African Rift is an active continental rift zone in eastern Africa that appears to be a developing divergent tectonic plate boundary where rift tectonism is accompanied by intense volcanism. The rift is a narrow zone in which the African plate is in the process of splitting into two new tectonic plates (McCall, 1967). It runs from the Afar Triple Junction in the Afar depression southward through eastern Africa. The East African Rift System consists of two main branches; the Eastern Rift Valley and the Western Rift Valley. These resulted from the actions of numerous normal (dip-slip) faults which are typical of all tectonic rift zones (Strecker et al., 1990).

The Kenya Rift Valley comprises 14 geothermal prospects (Figure 1) starting from Barrier in the north to Lake Magadi in the south (Omenda, 2000). It forms a classic graben with an average width of 40-80 km, dotted by several tertiary volcanoes. The rift floor is comprised mainly of the eruptive materials from these volcanoes (McCall, 1957). Most of the volcanic centres have gone through one

or more explosive phases including a caldera collapse. Some centres are dotted with hydrothermal activity and are envisaged to host extensive geothermal systems which are driven by still hot magma at shallow depths in the crust (Dunkley et al., 1993).

Menengai Volcano is of late Quaternary age which produced trachyte and pantellerites volcanics (McCall, 1957). Most of the surfaces adjacent to Menengai caldera is covered by extensive pyroclastics which accompanied the collapse of the caldera, with post caldera lavas mainly confined to the caldera floor and only one flow outside the caldera. Pre-caldera rocks are exposed on the face of the caldera cliff wall (Lagat et al., 2010).

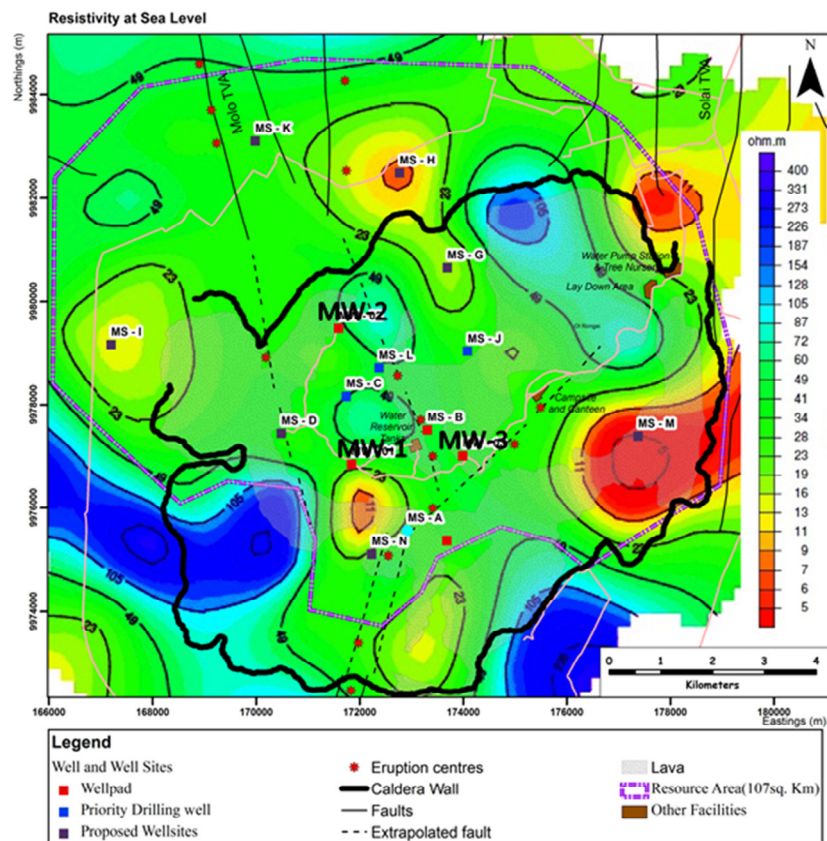


FIGURE 2: Resistivity distribution at sea level, showing also well sites MW-1, MW-2 and MW-3 (Lagat et al., 2010)

Pre-caldera rocks are exposed on the face of the caldera cliff wall (Lagat et al., 2010).

The main structure is the caldera itself which is elliptical in shape presenting a ring structure which is thought to be disturbed by the Solai graben faults on the northeast end and a fracture system at the south-southwest end (Strecker et al., 1990; Lagat et al., 2010). Other structures are the Ol-Rongai structural system which represents a part of the larger Molo Tectono-Volcanic Axis (TVA) and the N-S Solai tectonic axis which is a narrow graben averaging 4 km in width. More than 70 post-caldera lava flows cover the caldera floor, with some only a few thousand years old (Leat, 1985). Most of the caldera lavas are fissure eruptions which might have filled fracture openings (Lagat et al., 2010). The two tectonic volcanic axes may be extending into the caldera.

To the northwest of Menengai caldera lie the Ol-Rongai and Ol-Banita calderas which are thought to be older than the Menengai caldera, due to the presence of ignimbrite deposits which are older than the lava pile of the embryonic stage of Menengai (Lagat et al., 2010).

1.2 Hydrogeology and surface drainage systems

The surface drainage system is largely from the east and the western scarps. On the rift floor, the drainage is mainly from Menengai caldera northwards with the exception of the drainage from the southern rim or slopes of Menengai caldera into Lake Nakuru (Kuria and Woldai, 2003). The N-S, NE-SW, and NW-SW trending fault/fracture systems provide underground channels resulting in stream water disappearing underground. Hydrogeological information acquired from borehole data presented by Lagat et al. (2010) categorises the shallow hydrology system around Menengai into four classes: High yielding boreholes mainly hosted in fractured fresh lavas; moderately high yield boreholes hosted in lacustrine beds; reworked volcanoclastics and fractured lavas and boreholes hosted

in interbedding contacts between tuff and ignimbrite beds with poor yield; and dry and thermally anomalous boreholes mainly along the main structural axes.

1.3 Project scope

As part of the geothermal resource exploration strategy, the Geothermal Development Company (GDC) began drilling several deep wells in Menengai geothermal field. Drilling started in February 2011; at the time of writing this report, the first three wells are still undergoing various testing procedures, and drilling of the fourth well is underway. The results of downhole temperature and pressure measurements for wells MW-1, MW-2 and MW-3 will be discussed. An injection test conducted in MW-2 and a discharge test in MW-1 were analysed, although the discharge test was still in progress at the time of writing this report. Preliminary findings will be discussed and presented in this report in terms of initial reservoir pressure and formation temperature, transmissivity and storativity and discharge characteristics of the wells. Finally, a preliminary resource assessment was carried out for the area within the Menengai caldera.

2. DRILLING IN MENENGAI

2.1 Drilling targets

Exploratory wells were sited at the areas supported by the findings from the surface exploration. Figure 2 shows the location of these drill sites. Wells MW-1 and MW-3 were sited close to the up flow zones proposed by the surface exploration, while MW-2 was sited a few hundred metres away from a major fault running NE-SW close to the western caldera rim.

2.2 Summary of the drilling history of the wells

Well MW-1 was spudded on 12th February, 2011 and completed on 1st of May, 2011. The well was drilled using GDC drilling rig 1. Drilling commenced with a 26" hole down to 80 m where the 20" surface casing was installed to 79.6 m. Next, a 17½" hole was drilled down to 400.5 m where a 13⅜" intermediate (anchor) casing was installed to 398.7 m. Then a 12¼" hole was drilled down to 752 m, with a static formation temperature test (SFTT) conducted at 700 m (Figure 3). The temperature at this depth was estimated to be 110°C, which was not sufficient for production casing to be done. Drilling then continued to 843 m, and then the well was cased to 842 m using a 9⅝" casing. After the casing depth, an 8½" hole was drilled and progressed well down to 2206 m, where the drill string got stuck. The well was eventually terminated at this depth. A 7" slotted liner was installed from 802 down to 2172 m, with a 23.5 m 7" blank liner at the top (inside the production casing). Well MW-1 was drilled with mud initially and later with water, aerated water and foam to its final depth. Partial circulation losses were encountered at 1247-1342 and 1739-1802 m, while partial to total circulation losses were encountered at 1077, 1988-2007, 2031-2059 and 2124 m.

Well MW-2 was spudded on 28th February, 2011 and completed on 2nd July, 2011. The well was drilled using GDC drilling rig 2. First, a 26" hole was drilled with mud and later water to 81 m where a 20" surface casing was installed to 80 m. Next, a 17½" hole was drilled with water and later aerated water and foam down to 403 m with a 13⅜" intermediate (anchor) casing set to 381.3 m. Then, a 12¼" hole was drilled with water and aerated water with foam down to 805 m where drilling was stopped for SFTT (Figure 3), which was conducted at 750 m, and a 9⅝" production casing was set to 790.5 m. An 8½" hole was drilled and progressed with aerated water and foam to the well's bottom at 3200 m. Finally, a 7" slotted liner was installed from 754 down to 3189 m, with a 23.5 m 7" blank

liner at the top section of the hole. Total loss of circulation loss was not encountered at any depth below 800 m.

Well MW-3 was spudded on 1st June, 2011 and completed on 11th September 2011. The well was drilled using GDC drilling rig 1. Drilling commenced with a 26" hole down to 81 m where a 20" surface casing was set to 79.8 m depth. Next, a 17½" hole was drilled with water and later with aerated water and foam down to 400 m and a 13¾" intermediate (anchor) casing was set to 397.5 m. Next, a 12¼" hole was drilled with aerated water and foam to 914.6 m and stopped for SFTT measurements which were conducted at 904 m. There was a slight increase in temperature, and then a drop as seen in the build-up data (Figure 3); thus, static temperature could not be estimated. The temperature fluctuations could be due to cold fluid at this depth. Drilling continued to 1100.5 m and the production casing was set to 1096.5 m. An 8½" hole was drilled with aerated water and foam down to 2112.5 m where the string got stuck while trying to pull out of the hole. The well was later terminated at this depth after trying to free the stuck string for close to one month. Total loss of circulation was encountered between 914 and 962 m and partial loss of circulation occurred between 966 and 1057 m (this section is cased off). Total circulation losses occurred immediately below the casing at 1107 m and partial loss of circulation was encountered between 1728 and 1813 m. A 7" slotted liner was installed from 1058 down to 2101 m.

2.3 Well programme

The three exploration wells MW-1, MW-2 and MW-3 are vertical wells drilled within the Menengai caldera. Table 1 gives a summary of the locations, well casing programmes and total drilled depth of each well.

TABLE 1: Well location and casing depth summary (well depth reference is ground level)

Well ID	Easting	Northing	Elevation (m)	Well depth (m)	Depth of 13¾" anchor casing (m)	Depth of 9¾" prod. casing (m)	Depth interval of 7" liner (m)
MW-1	171847	9976849	2051	2195	398.7	842	802-2172
MW-2	171598	9979482	1894	3189	381.3	791	754-3189
MW-3	173312	9977009	2058	2101.5	397.5	1096.5	1058-2101

3. DOWNHOLE MEASUREMENTS

Downhole measurements are conducted in geothermal wells to gain information on the physical characteristics of a geothermal reservoir. Temperatures and pressures are measured directly to obtain actual information on downhole conditions. Different tests and measurements are conducted and the findings are used for estimating properties such as permeability, storage capacity and other reservoir and formation properties. Downhole measurements and tests conducted in MW-1, MW-2 and MW-3 are discussed in the following subsections.

3.1 Static formation temperature tests (SFTT)

A static formation temperature test is usually conducted in the first exploration wells to derive an estimate of the formation temperature while drilling in order to determine the depth into which a production casing shoe can be set. The standard procedure is to set it at an appropriate depth to case off the entry of cool fluids into the well. Therefore, measurements are conducted at accepted interruptions during drilling. However, due to the cooling caused by circulating fluid, it is not possible

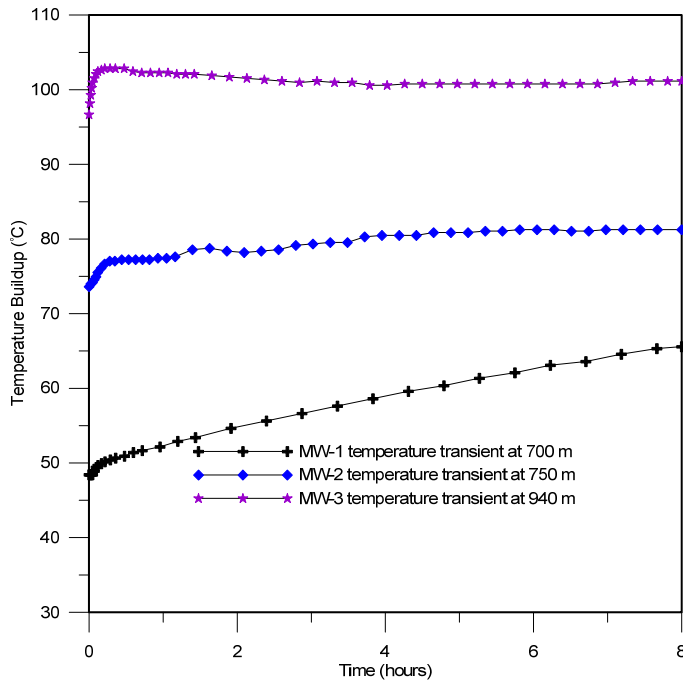


FIGURE 3: Temperature transient data for the exploration wells at SFTT depths

to measure the true formation temperature directly until months or years have passed as the system needs to stabilize, although it might be impossible due to boiling in the well, or fluid flow might screen the formation temperature (Helgason, 1993). The test is done by monitoring temperature build-up for at least eight hours at a predetermined depth (after allowing circulation for at least twelve hours). To ensure that only heat conduction governs temperature recovery, the test should be conducted at sections where there are no circulation losses (Roux et al., 1979).

Static formation temperature tests were carried out in the Menengai wells during approximately 13 hours of stopped drilling in each of the three wells. In well MW-1 the test was done at 700 m, at 750 m in MW-2 and at 904 m in MW-3. The tests were done by first measuring a

temperature and pressure profile to the maximum cleared depth. The purpose of this profile was to determine the temperature at the bottom of the hole. SFTT is not necessary if the bottom hole temperature is above 200°C. This was followed by stationing a mechanical Kuster pressure and temperature tool at the determined depth (in each well), for a duration of 8 hours, after which the tools were retrieved. Downhole temperature and pressure profiles followed, where the Kuster pressure and temperature tools were run and measurements made every 100 m in the production casing, then every 50 m to the well's bottom.

The build-up temperature data (Figure 3) obtained during the above tests (at the time when drilling was still in progress) were analysed using the Horner plot method, but different from the conventional technique as a correction factor was applied as presented in Roux et al. (1979).

Temperature build-up data obtained during the SFTT during drilling (presented in Figure 3) were also analysed using the Albright method, which is one of the two methods employed in the BERGHITI program which was developed at ISOR. As discussed by Helgason (1993), the Albright method assumes that for an arbitrary time interval, much shorter than the total recovery time, the rate of temperature relaxation depends only on the difference between the borehole temperature and the formation temperature. If the logging time is represented as $I = (t_1, t_N)$, where N is the number of data points in the log, then for any time interval $i \in I$, $i = (ta, tb)$, we find $\forall t \in i$, the θ_∞^i , c^i and θ_0^i give us the best solution to Equation 1 below:

$$e^{c^i t} = \frac{\theta_\infty^i - \theta(t)}{\theta_\infty^i - \theta_0^i} \tag{1}$$

- where $\theta(t)$ = The temperature at time t , $t \in i$;
- θ_∞^i = The estimated formation temperature for the time interval I ;
- θ_0^i = The estimated temperature at the circulation stop; and
- c^i = A constant.

Formation temperature is then determined by plotting c^i as a function of θ_{∞}^i . As shown in Figure 4 below, the formation temperature is the value $\theta(t)$ when $t \rightarrow \infty$. Formation temperatures were estimated as 170°C and 108°C for MW-1 and MW-2, respectively. Temperature measurements in MW-3 could not be used for estimating the formation temperature due to temperature fluctuations during the build-up period. At the beginning, the temperature increased slightly by 6°C, then decreased slightly, followed by a slow recovery. Since the well was drilled to 914 m, and SFTT was conducted at 904 m, fluctuations in the temperature recovery can be attributed to disturbances by cold fluid at this depth, resulting in conductive cooling.

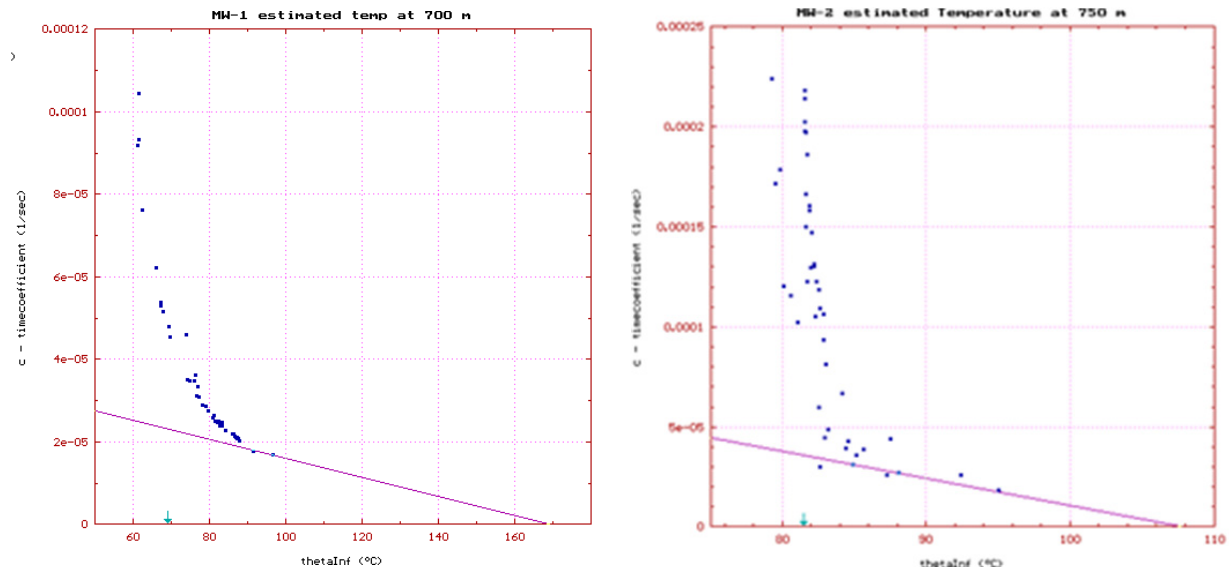


FIGURE 4: Estimated formation temperatures (Albright's method) for MW-1 and MW-2 at 700 and 750 m, respectively

3.2 Temperature and pressure profiles

The formation around the wellbore cools down as a result of drilling and pumping during a completion test. In impermeable horizons, conductive cooling takes place, whereas in permeable zones, quenching occurs as water permeates the formation (Stefánsson and Steingrímsson, 1990; Grant, 1979). Monitoring the temperature recovery after drilling unmasks several characteristics of the well, thus mirroring the reservoir condition. This is possible because the fluid is dynamic during the process and, until it attains a stable condition, will reveal the state of the fluids penetrated by the well in the reservoir. Conduction and convection govern the heat transfer between the rock and the fluid, with conduction taking place in impermeable horizons and convection prevalent in permeable zones (Bodvarsson and Witherspoon, 1989; Grant and Bixley, 2011). Convection processes greatly outweigh conduction as a means of heat transfer. In temperature logs during injection, a loss (in flow) of fluid is seen as a slight change in the gradient of the temperature profiles, whereas fluid gain is reflected by a sudden jump in temperature (Stefánsson and Steingrímsson, 1990). Wells with poor permeability are commonly very slow in heating up, while permeable wells with strong internal flow are heated up in only a few hours or days. The zone that accepts the bulk of the fluid during injection may take a longer time to warm up and generally recovers during the stabilization period. Some of the prominent features observed in the wells during heat-up are profiles approaching or corresponding to the boiling point curve of water associated with up-flow areas; down flowing fluids suggesting isothermal profiles from a feed point to the exit point; profiles showing temperature reversals which are common in outflow areas; and linear temperature gradients in impermeable zones.

Pressure logs are used to identify the horizons that control well pressures, usually the feed zones. As discussed by Grant and Bixley (2011), there is a direct contact between the well and the reservoir at the feed zones such that the well pressure equals the reservoir pressure at this point, referred to as the pivot point of a well. During the heat-up period, wellbore fluid changes temperature and, thus, the density of the fluid shifts, resulting in a change in the pressure gradient (Renner et al., 2007). Where the separate pressure profiles converge is the pivot point. As discussed by Grant and Bixley (2011) and Stefánsson and Steingrímsson (1990), pressure at the feed zone remains fixed by the formation pressure, so the pressure profiles of wells with one feed pivot around the feed depth. In a well with several feed zones, the pivot will form at a depth between the different feed zones of the well and normally closer to the strongest feed.

3.2.1 MW-1 profiles

Figure 5 shows temperature logs from MW-1 during the heating-up period. The first log was done four hours after drilling, while the other temperature logs were subsequent to this heating-up period, after drilling (static) and during the flow testing of the well (dynamic logs). The dashed curve shows the boiling point curve which is derived by assuming that the water column in the well is at boiling point temperatures from the water level down to the bottom of the well, while the solid curve shows the estimated formation temperature based on measurements in the well.

A temperature profile taken 4 hours after drilling indicated a temperature reversal from around 1200 m to the well bottom as a result of cooling during drilling. Heating profiles indicated feeds (inflows) at around 1050 m, and below 1250 m. The feed zones below 1800 m contribute hotter fluid than the upper feeds as seen on the 01.06.2011 flowing profile, contributing over 260°C fluid as the fluid boils before flowing into the well. Up flowing fluid cools as it rises up the wellbore due to boiling and mixing with more gassy fluids contributed by the upper feeds. Significant shift was observed between

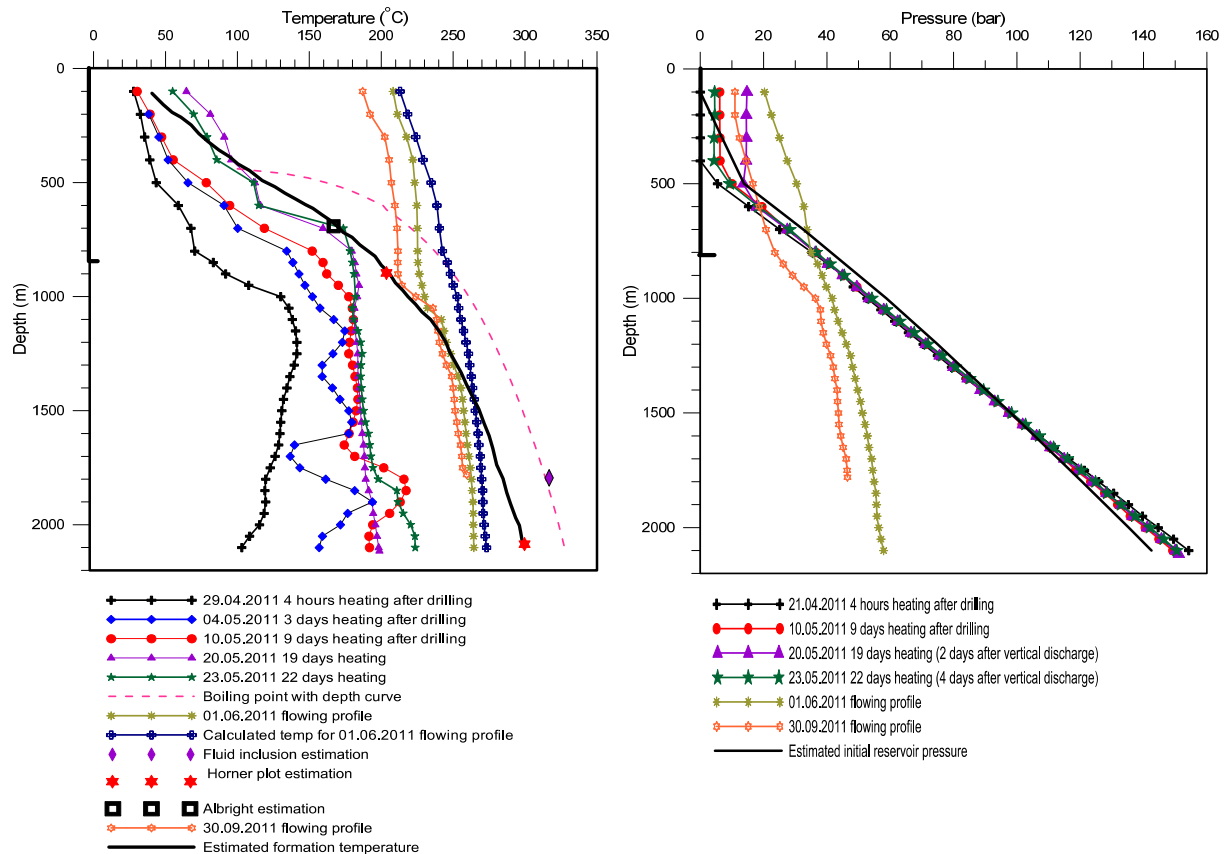


FIGURE 5: MW-1, temperature profiles with estimated formation temperature (left), and pressure profiles with estimated initial reservoir pressure (right)

1050 and 1100 m, which may be a result of inflow of fluid containing significant amounts of gas into the well and mixing with the hot two-phase fluid as it flows up the wellbore. Comparison of the computed flowing temperature from the flowing pressure on 1.06.2011 and the 1.06.2011 flowing temperature profile presents a significant shift which is most likely due to presence of gas in the two-phase flow. Pronounced shift above 1100 m indicates additional gas getting into the well from the feed at this depth, shifting the boiling point. The 30.09.2011 flowing profile also indicated boiling fluid with a similar shift from the calculated profile, due to the effects of gas.

Figure 5 also shows pressure profiles in well MW-1. The profiles indicate a water level at around 440 m below the surface. Heat-up pressure profiles present a pivot point at around 1500 m. The heat-up profiles were obtained only up to a maximum of 22 days of heating; therefore, future shut-in pressure profiles might show the pivot depth in the well more clearly. The major feeds in the well occur at around 1050, 1800 and 2050 m, with the pivot point occurring in between these feeds. The flowing pressure profiles indicate boiling of two-phase fluid all the way from the well bottom. The presence of a significant amount of gas in the well caused a shift of the boiling point of the water.

3.2.2 MW-2 profiles

Figure 6 shows temperature profiles during drilling, during injection and heating-up in MW-2. The solid curve shows the estimated formation temperature. The profile taken while pumping (30.06.2011) shows that the injected water flows down the well, with a minor loss zone at around 1150 m, evidenced by a slight change in the gradient. At around 2250 m hot fluid enters the well resulting in an instant jump. The mixture then flows down, exiting at a loss zone at around 3000 m. Heat up profiles indicated a hot section between around 1000 m and 1300 m, which is probably due to a shallow hot system. Below 1300 m a cold section was found, due to cold fluid influx into the well at around this depth, flowing down and masking temperatures at minor feeds down to around 2250 m. A consistent jump in temperature below 2250 m found in all the heat-up profiles was due to hotter fluid entering the well, mixing with the colder fluid and then exiting at around 3000 m. Initial slow recovery below 2250 m was observed but the cold fluid flow from above slowed the heating up process and, eventually, effectively cooled the well to the bottom, as evidenced by the 17.08.2011 and 16.09.2011 profiles.

Pressure profiles indicated a water level at 300- 400 m. Heat-up pressure measurements did not show any pivot point in this well. The density of the fluid in the well increased with time, increasing the pressure gradient inside the well.

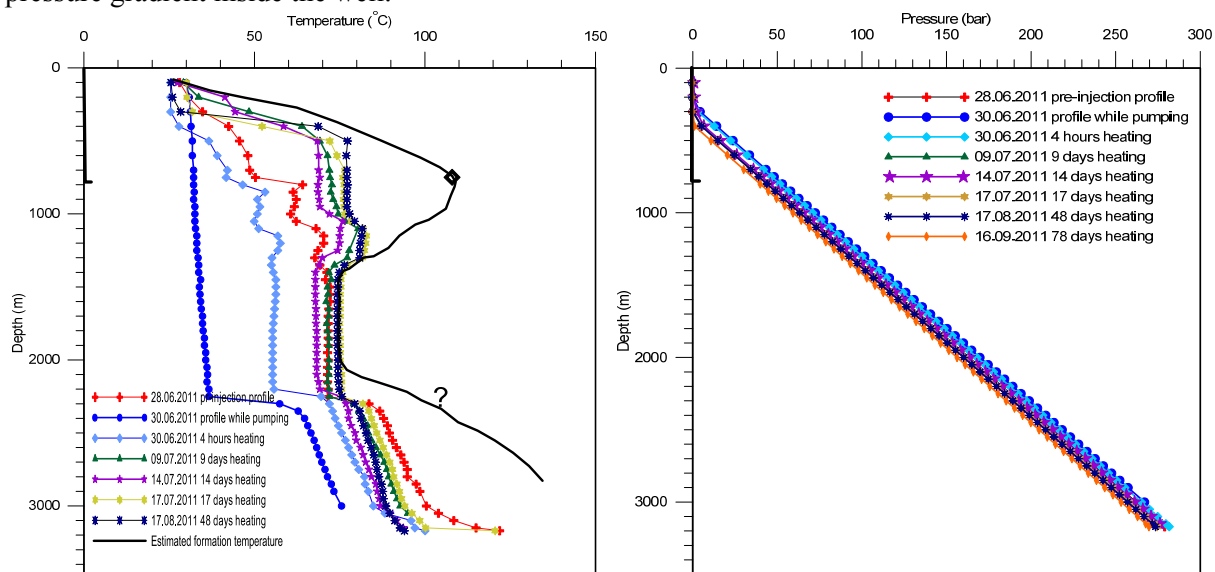


FIGURE 6: MW-2, temperature (left) and pressure (right) profiles with estimated formation temperature

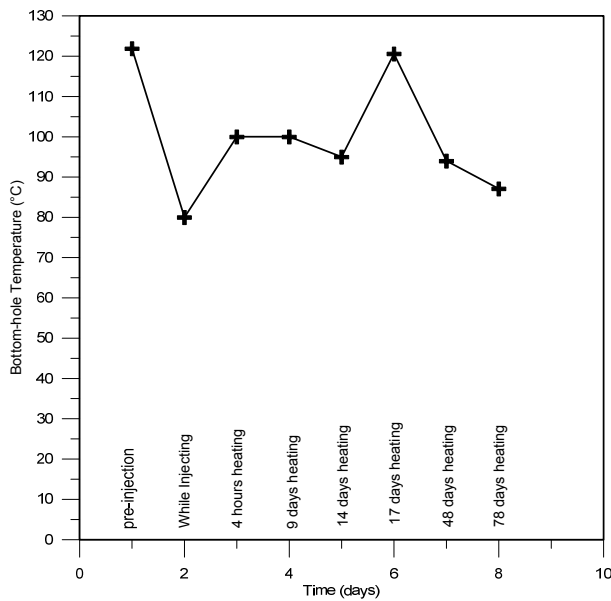


FIGURE 7: Variation of MW-2 bottom-hole temperature with time

Variations of MW-2’s bottom hole temperature with time are presented in Figure 7. A temperature log after drilling presented a bottom-hole temperature of over 120°C. Injection into the well cooled the bottom down to 75°C. Subsequent heat-up logs showed the well-bottom was slowly recovering up to around 100°C after 9 days of heat-up. After 14 days, the well bottom had cooled down to 95°C, but then heated up to 120°C after 17 days of heat-up. Bottom temperature after 48 and 78 days indicated that the well bottom was cooling due to the down-flow from upper feeds.

3.2.3 MW-3 profiles

The drilling of well MW-3 was completed on 11th September, 2011. Well MW-3 temperature logs are shown in Figure 8. Heating profiles in this well showed a cold section between 1250 and 1550 m, indicating that the main permeability structures intersected by the well are in this interval. Profiles after 14 and 22 days still showed cooling at this section (between around 1250 and 1550 m). Below 1600 m there is a conductive section, with a slight change in the gradient at the bottom, probably due to a minor feeder.

Pressure profiles indicated a water level around 400 m. They also presented a probable pivot point at around 1450 m, indicating that a major permeable zone is close to this depth. Future pressure profiles might define this pivot point more clearly.

Pressure profiles indicated a water level around 400 m. They also presented a probable pivot point at around 1450 m, indicating that a major permeable zone is close to this depth. Future pressure profiles might define this pivot point more clearly.

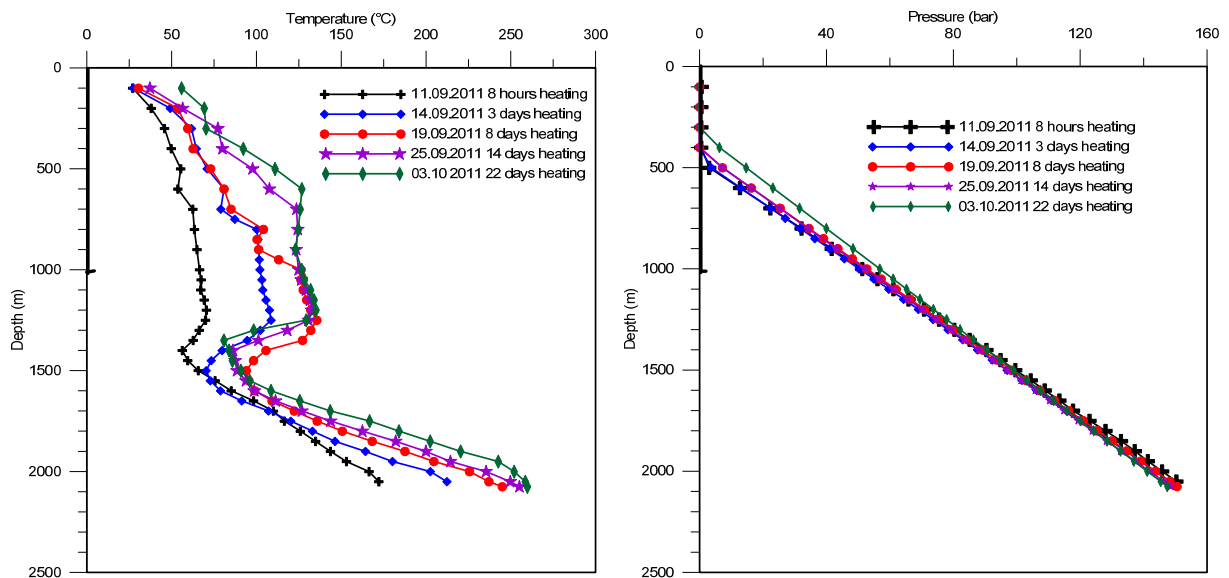


FIGURE 8: MW-3, temperature (left) and pressure (right) profiles during the heat-up period

3.3 Estimation of formation temperature and initial reservoir pressure

Formation temperatures serve as a base for conceptual models of geothermal reservoirs and are also important for making decisions upon well completion (i.e. to decide on casing depths). The Horner plot was used for analysis of recovery data from wells MW-1 and MW-2 in order to estimate the

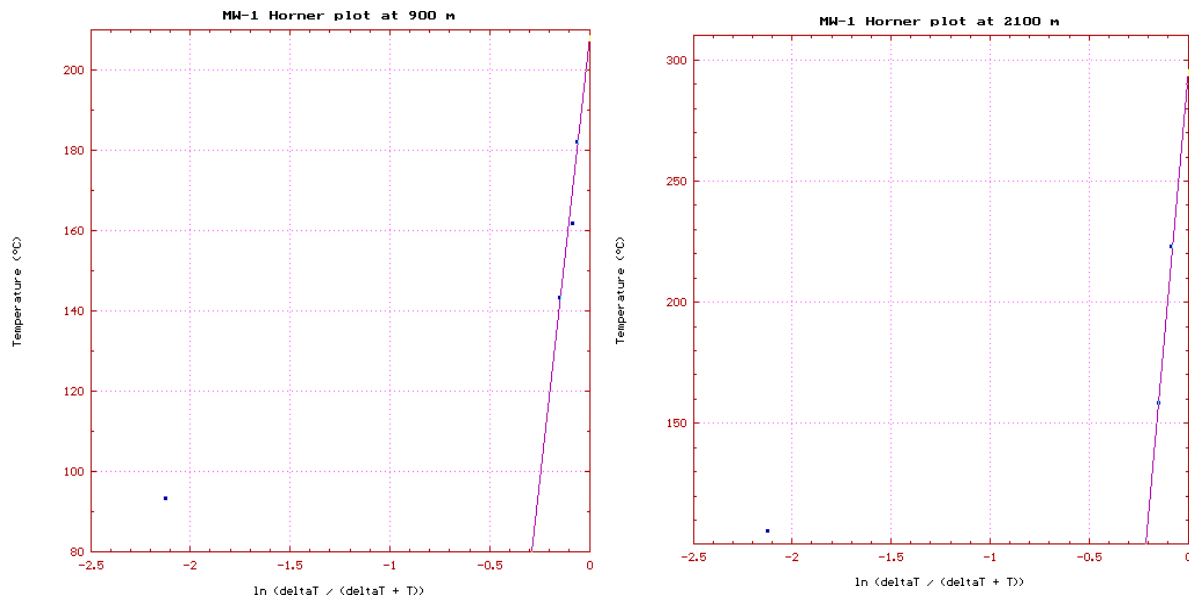


FIGURE 9: MW-1 estimated formation temperature using the Horner plot method for the heat-up data at 900 m (left) and 2100 m (right)

formation temperature. Temperatures at 900 and 2100 m depths in MW-1 were estimated using the Horner plot method; however, as a result of the cooling in MW-2, formation temperature estimation using this method was not possible. The estimated formation temperature is shown with solid curves in Figures 5 and 6.

All the temperature profiles in well MW-1 were analysed in order to estimate the formation temperature profile, including Horner plots. Additional information was obtained from the SFTT test at 700 m during drilling, and also from fluid inclusion sections. The temperature estimates using the Horner plot of the heat-up period data at 900 and 2100 m (Figure 9) are 208 and 298°C, respectively. The result of the analysis is the formation temperature profile in Figure 5. It shows a conductive profile down to around 800 m where the formation temperature is estimated at close to 200°C. Temperature continued to rise below 800 m as it became more convective, reaching close to 300°C at the bottom (2100 m). The formation temperature profile estimated from the available data has a similar shape as the boiling point curve but it is cooler. A fluid inclusion study on well cuttings from MW-1 at 1800 m presented trapped fluid in quartz crystals at a homogenization temperature of over 320°C (Omondi, 2011). This indicates the possibility of boiling temperatures at around this depth. It is quite possible that the formation temperature is underestimated from the present data, but future shut-in temperature logs should give a more accurate estimation of the temperature conditions around MW-1. The initial reservoir pressure was estimated using the ICEBOX program PREDYP, where the water level in the well was varied until a match of pressure at the pivot (1500 m) was obtained.

MW-2's estimated formation temperature at the upper section (from the surface to around 750 m) showed a conductive gradient (SFTT indicated temperatures of over 100°C at 750 m depth). The section between 1400 and 2200 m seemed to have more or less attained thermal equilibrium; therefore, the formation temperature is thought to be stable between these depths. Below 2250 m, the temperature recovery was disturbed by the down flowing cold fluid from the upper section; otherwise, the temperature could be higher than the highest temperature recorded immediately after drilling. Estimating temperature at the cooled sections was challenging.

3.4 Main feed zones

Feed zones are regions in the well where direct communication with the reservoir occurs. Identification of these regions defines the entry and exit points of fluids into or out of the wells.

Therefore, determining the suitability of wells as production or injection wells, starts with having feeders. Information on the depths of main feed zones also serves as an input in conceptual models of geothermal reservoirs.

Table 2 below presents the location of feed zones as identified through temperature logs during heat-up and pivot points observed in pressure profiles. Depths where circulation losses were recorded are also indicated. By combining the information on the feed zones identified during heat-up and information on circulation losses, it can be observed that the main feed zones for MW-1 at around 1050, 1800 and 2050 m can be related to the loss of circulation experienced at around these depths. Only partial circulation losses were recorded in MW-2, making comparison difficult. MW-3 circulation loss zones, however, could not be tied to the feeds identified from temperature logs during heat-up.

TABLE 2: Temperature and pressure logs feed zones depths and circulation loss depths below the casing for MW-1, MW-2 and MW-3

Well ID	Total depth (m)	Circulation loss depth (m)	T-logs – approx. feed depth (m)	Pivot point depth (m)
MW-1	2195	1077, 1247-1342, 1739-1802, 1842-1843, 1988-2007, 2031-2059, 2124	1050, 1250, 1800, 2050	1500
MW-2	3189	Partial losses	1150, 1300, 2250, 3000	Not observed
MW-3	2101.5	1057, 1107, 1728-1813	1250, 2050	Not observed

It should be remembered that regions where loss of circulation was experienced during drilling are not necessarily feed zones. Therefore, it is important to combine circulation loss data with heat up temperature and pressure logs in order to find circulation loss zones which coincide with actual feed zones.

4. INJECTION WELL TEST

4.1 Introduction

After successful drilling of geothermal wells, well testing is conducted in order to evaluate the conditions of the well in terms of flow capacity and reservoir properties. Geothermal wells, unlike groundwater and petroleum wells, are not clearly defined geologically. The permeability structure of a geothermal aquifer is independent of geological boundaries (Grant and Bixley, 2011). Therefore, the thickness is not really known, nor is the porosity or fluid properties. Separate parameters, k (permeability), h (thickness), ϕ (porosity), μ (viscosity) cannot be measured directly, but transmissivity and storativity are possible to identify. These properties are of utmost importance since transmissivity controls the ability of the reservoir to deliver fluid, and storativity the mass of fluid that is released; permeability thickness and storativity control the overall pressure variations and fluid flow in geothermal reservoirs (Axelsson, 2011).

4.2 Theoretical background

During an injection test, the response of a reservoir to changing injection is monitored. A change in the flow rate usually results in changes in pressure which can be measured. Since the response is characteristic of the properties of the reservoir, it is possible in many cases to infer reservoir properties from the response (Horne, 1995). Reservoir properties are not evaluated directly from the data, but are

interpreted with the most appropriate model resulting in average values (Horne, 1995, Grant and Bixley, 2011). The pressure diffusion equation is the basis for all models and is the most used equation in well test theory. The most used solution to the pressure diffusion equation is the Theis solution. The pressure diffusion equation is derived from the conservation law of mass along with Darcy's law and the equation of the state of the fluid, as presented by Horne (1995) and Jónsson (2011).

4.2.1 Pressure diffusion equation

Considering a cylindrical control volume around the well and applying conservation of mass (Equation 3):

Mass flow in – mass flow out = mass rate change within the control volume

$$\left[\rho Q + \frac{\partial(\rho Q)}{\partial r} dr \right] - \rho Q = 2\pi r dr \frac{\partial(\varphi \rho h)}{\partial t} \quad (3)$$

Darcy's law (conservation of momentum):

$$Q = \frac{2\pi r h k}{\mu} \frac{\partial p}{\partial r} \quad (4)$$

where ρ = Density of the reservoir fluid;
 Q = Flow rate;
 r = Distance (radius);
 φ = Porosity of the reservoir rock;
 h = Effective reservoir thickness (m);
 t = Time since well test started;
 k = Permeability of the rock matrix (m²);
 μ = Dynamic viscosity of the fluid (Pa·s).

Fluid and reservoir compressibility:

$$\text{Fluid compressibility} \quad c_w = \frac{1}{\rho} \frac{\partial \rho}{\partial p}$$

$$\text{Rock compressibility} \quad c_r = \frac{1}{1 - \varphi} \frac{\partial \varphi}{\partial p} \quad (5)$$

$$\text{Total compressibility} \quad c_t = \varphi c_w + (1 - \varphi) c_r$$

Combining Equations 3, 4 and 5 results in the pressure diffusion equation (Equation 6):

$$\frac{\partial^2 p}{\partial r^2} + \frac{1}{r} \frac{\partial p}{\partial r} = \frac{\mu c_t}{k} \frac{\partial p}{\partial t} = \frac{S}{T} \frac{\partial p}{\partial t} \quad (6)$$

where $T = \frac{k h}{\mu}$ = Transmissivity (m³/Pa·s);
 S = Storativity (m/Pa).

The Theis solution (line source solution) is an integral solution of the above pressure diffusion equation (Earlougher, 1977; Horne 1995; Jónsson, 2011). It is obtained with the assumptions that the reservoir is infinite and the radius of the wellbore is negligible. The initial and boundary conditions used are:

Initial condition: $p(r,0) = p_i$ for all $r > 0$

Boundary conditions:

At infinity: $\lim_{r \rightarrow \infty} p(r,t) = p_i$ for all $t > 0$

At the well: $Q = \frac{2\pi kh}{\mu} \lim_{r \rightarrow 0} \left[r \frac{\partial p}{\partial r} \right]$ for all $t > 0$

The solution to the radial pressure diffusion Equation (Equation 6), $p(r,t)$, is then:

$$p(r,t) = p_i + \frac{Q\mu}{4\pi kh} Ei \left[-\frac{\mu c_t r^2}{4kt} \right] \quad (7)$$

Ei is the exponential integral defined as:

$$Ei(-x) = - \int_x^{\infty} \left(\frac{e^{-u}}{u} \right) du \quad (8)$$

For small values of $x = \frac{Sr^2}{4\pi T}$, i.e. $x < 0.01$, we can use:

$$Ei(-x) \approx + \ln(x) + \gamma$$

where $\gamma = 0.5772$ is the Euler's constant.

Therefore, if $t > 100 \mu c_t r^2 / 4kt$ and using $\ln(x) = 2.303 \log(x)$, the solution for the radial pressure diffusion equation can be simplified to:

$$p(r,t) = p_i + \frac{2.303Q\mu}{4\pi kh} \left[\log \left(\frac{\mu c_t r^2}{4kt} \right) + \frac{\gamma}{2.303} \right] \quad (9)$$

Equation 9 describes isothermal flow of a fluid in a porous media, i.e. how the pressure (p) diffuses radially through the reservoir as a function of the distance (r) from the well and the time (t) since the start of production, $p = p(r,t)$. Initial and boundary conditions are needed to find the solution in a particular case. The simplifying assumptions on the reservoir and flow used are:

- Darcy's law applies; reservoir is considered homogenous and isotropic and the well fully penetrates the entire formation thickness;
- Flow is considered isothermal;
- Porosity, permeabilities, viscosity and compressibilities are constant;
- Fluid compressibility is small;
- Pressure gradients in the wells are small; and
- Flow is single phase.

4.2.2 Semi-logarithmic analysis

This solution can be written for constant distance r as:

$$p_i - p(r,t) = \frac{2.303Q\mu}{4\pi kh} \left[\log \left(\frac{4k}{\mu c_t r^2} \right) - \frac{\gamma}{2.303} \right] + \frac{2.303Q\mu}{4\pi kh} \log(t) \quad (10)$$

This equation is in form of $\Delta p = A + m \log(t)$, which is a straight line with slope m on a semi-log graph where:

$$\Delta p = p_i - p(r, t); A = \frac{2.303Q\mu}{4\pi kh} \left[\log \left(\frac{4k}{\mu c_t r^2} \right) - \frac{\gamma}{2.303} \right]; m = \frac{2.303Q\mu}{4\pi kh}, \text{ with units Pa/unit cycle.}$$

When pressure change (Δp) is plotted against time, t , on a semi-logarithmic scale, (Δp vs. $\log t$), an asymptotic straight line response for the infinite acting radial flow period of a well is obtained. Once the slope, m , has been identified, the transmissivity, T , can be calculated by Equation 11:

$$T = \frac{kh}{\mu} = \frac{2.303Q}{4\pi m} \quad (11)$$

In a case where the temperature is known, the dynamic viscosity, μ , can be inferred from steam tables, and the permeability thickness, kh , may be calculated using Equation 12:

$$kh = \frac{2.303Q\mu}{4\pi m} \quad (12)$$

The formation storativity or storage coefficient, $S = (c_t h)$ is then obtained from the intercept with the Δp -axis when the permeability thickness is known. Storativity (S) can be computed from Equation 13, using the value of the drawdown, Δp , at some time, t :

$$S = 2.246T \left(\frac{t}{r^2} \right) \cdot 10^{\frac{-\Delta p}{m}}, \text{ where } T = \frac{kh}{\mu} \quad (13)$$

The early pressure data are often affected by wellbore and skin effects. Wellbore storage causes the reservoir flow rate to differ from the wellhead rate; it is most pronounced at the early time and becomes negligibly small at later time (Horne, 1995; Bodvarsson and Witherspoon, 1989; Johnson and Lopez, 2003).

4.2.3 Horner plot method for pressure recovery

This method is based on the line source solution to diffusivity and applies to fall-off preceded by a constant rate injection period. Pressure fall-off data are often plotted as a function of $\log ((t + \Delta t)/\Delta t)$, where t denotes the injection time and Δt is the shut-in time. A data plot asymptotically approaches a straight line with the slope obtained by the pressure change over one log circle (Garg and Pritchett, 1989). The slope may be used to compute transmissivity by using the semi-logarithmic equation for finding transmissivity.

4.3 MW-2 Injection test analysis

No injection test data were available from well MW-1, but injection data from well MW-2 were analysed. The injection test in MW-2 consisted of injecting cold water at varying rates into the well and simultaneously recording the pressure and downhole temperature over a 13 hour period. Pre-injection pressure and temperature were measured to select the appropriate point to station the pressure and temperature tool during the test. The pressure and temperature tool was placed at 2500 m. Injection was done in steps (Figure 10): starting with 16.7 l/s for 4 hours, increasing to 21.7, 26.7 and eventually 31.7 l/s, for a total of 13 hours altogether. A profile, while pumping at the maximum rate (31.7 l/s), was then conducted, followed by placing the pressure and temperature tool at the initially selected depth and monitoring pressure fall-off for 8 hours (Figure 11).

The MW-2 injection test was analysed by utilizing both the WellTester software and graphical methods. The WellTester program was developed at ÍSOR - Iceland GeoSurvey to handle and analyse well test data. A reservoir model was specified, based on the type of response observed from the derivative plot. As discussed by Tiab (1975), a log-log plot of pressure derivative versus time is

important in identifying flow regimes and boundary effects. The reservoir properties that the model relies on were then calibrated until a good fit was seen between the measured pressure transient and the theoretical pressure transient (Júlíusson et al., 2007). An injection test analysis by semi-log analysis was also conducted by using graphical presentations using approximations that are often associated with log (time) behaviour (i.e. infinite acting radial flow). The WellTester program utilizes type-curves which combine both pressure and pressure derivative functions during analysis.

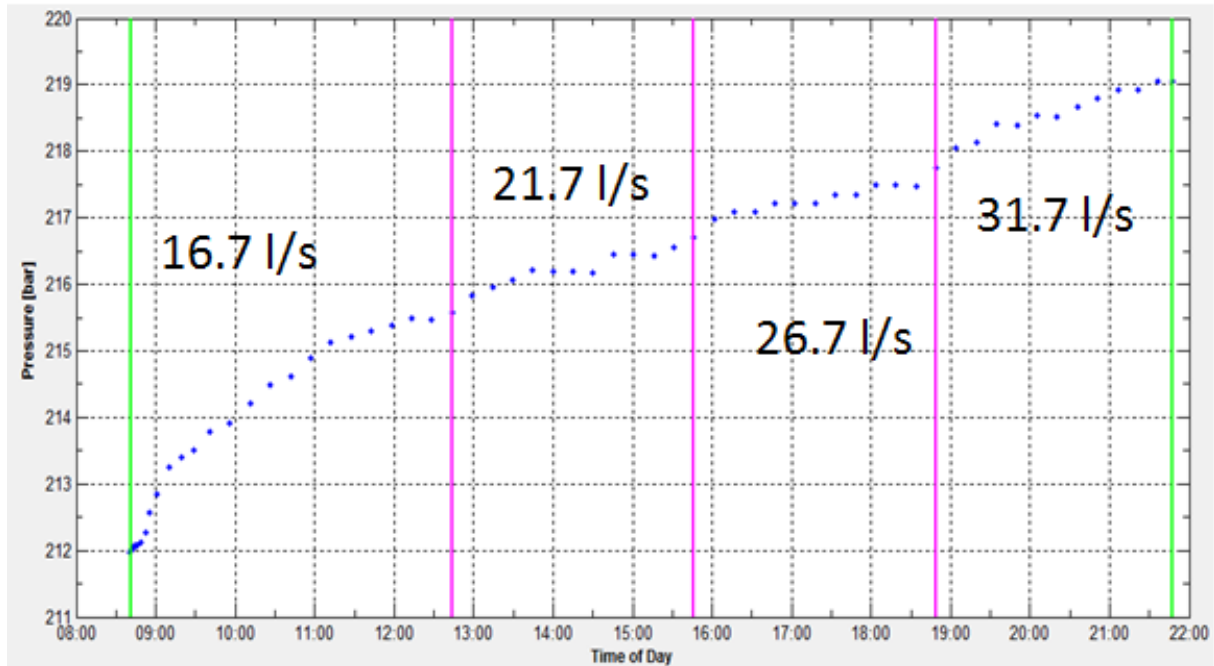


FIGURE 10: MW-2 injection steps for a duration of 13 hours with respective pumping rates at each step

After injecting for thirteen hours at a variable rate, 7 bar of pressure build-up was recorded. The rapid initial pressure rise was followed by slow and fluctuating pressure build-up (Figure 10), making the pressure data challenging for inferring formation transmissivity. It is possible that water flow rates were fluctuating during the injection steps which would explain the unstable pressure response that was recorded. It is also evident from the steps that the injection duration was short, especially for the last three steps, since the radial flow regime was not observed. Pressure fall-off data (Figure 11) were, therefore, utilised for inferring reservoir properties. The semi-log plot of pressure fall-off data presented a slope, m of 0.5 bar/cycle for the early time data. The straight line on the semi-log plot

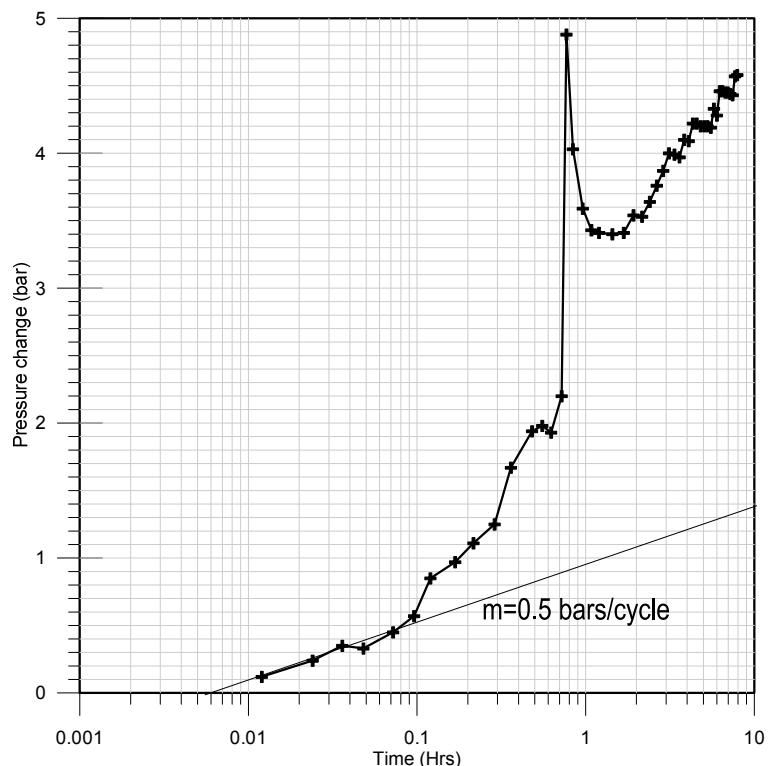


FIGURE 11: Semi-log plot for MW-2 pressure fall-off data

cuts $\Delta p = 0$ at time $t_0 = 0.006$. From these values, MW-2 transmissivity was estimated at $11.7 \times 10^{-8} \text{ m}^3/\text{Pa}\cdot\text{s}$, while its storativity was estimated at $1.58 \times 10^{-7} \text{ m/Pa}$.

An effort was made to clean the data before using the WellTester program. Considering the nature of the trends presented by the derivative plots for all steps and comparing those with the boundary cases, a homogenous reservoir with constant pressure boundary, constant skin and wellbore storage was the model considered for well MW-2. Non-linear regression was performed to find the parameters that best fit the data. Out of the four steps, step 1 presented a fairly good fit. The results from the analysis are presented in Figure 12.

Although the fit obtained for the first step is not an exact match, the transmissivity value obtained ($8.56 \times 10^{-8} \text{ m}^3/\text{Pa}\cdot\text{s}$) and the storativity value, $1.48 \times 10^{-7} \text{ m/Pa}$, are comparable with that computed by the semi-log method for the fall-off data. The change in the injection flow over the change in stabilized injection pressure gave an Injectivity Index (II) ranging between 4.18 and 4.51 l/s/bar.

The pressure response during injection steps is sensitive to any fluctuations in the water flow rates. Maintaining a steady flow rate throughout the injection period ensures stable pressure transient data which, when analysed and fitted to models, gives properties that accurately infer reservoir properties. The injection steps should also be long enough to enable seeing the radial flow section which is interpreted to give the reservoir property of transmissivity.

5. DISCHARGE TEST

Once a well has heated up after drilling, a discharge test is conducted to estimate its production potential. A discharge test is conducted by starting the well's flow and taking measurements to evaluate the mass flow, fluid enthalpy and chemical characteristics of the fluids (Bodvarsson and Witherspoon, 1989). The first step in flow testing is starting well discharge. Most wells naturally develop sufficient pressure of either cold gas or steam, so that opening the control valve automatically initiates flow. But it is difficult to start flow in some wells, even after waiting for weeks for the well to heat up following drilling. This is because, in such cases, no pressure develops at the wellhead. This problem is most common in fields that are under-pressured or where there is a cold section in the upper part of the wellbore (Grant and Bixley, 2011). The production of steam and water from a

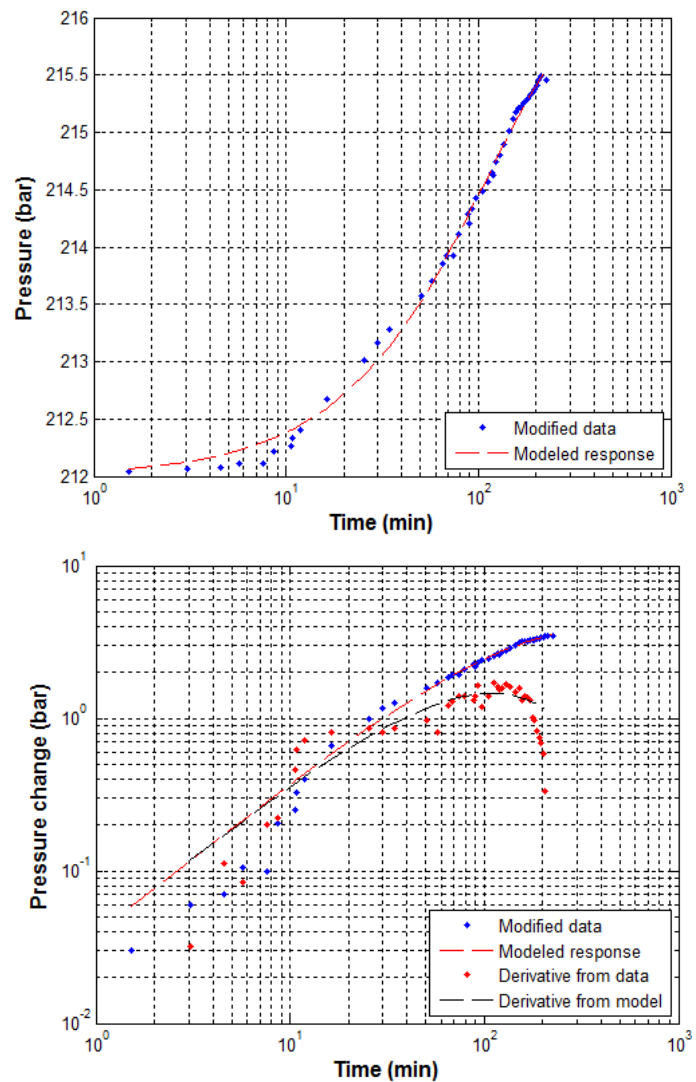


FIGURE 12: Fit between model and collected data for step number 1, using a logarithmic time scale (above); on a log-log scale (below)

geothermal reservoir depends on the reservoir pressure, the flow of fluid through the feed zone into the well, and then up the wellbore to the surface.

5.1 Lip pressure method

The Lip pressure method, which is based on an empirical formula developed by Russell James, was utilised for interpreting flow measurements in MW-1. This method is described by Grant et al. (1982) and by Grant and Bixley (2011). The steam-water mixture is discharged through a straight pipe of known diameter into a silencer to separate the steam and water phases at atmospheric pressure. The silencers used are lined with pumice to reduce the noise level produced by the discharge. The lip pressure is measured at the extreme end of the discharge pipeline as it enters the silencer, and the separated water flow exiting from the silencer is channelled into a sharp-edged weir, where the height above the V-notch is measured. The steam exits at the top of the silencer and discharges into the atmosphere. Using the measured parameters, wellhead pressure, lip pressure, and the height of the water over the V-notch, flow enthalpy and the total mass flow rate were calculated using a quick basic program – BASICA which was developed from the James equation which relates mass flow, enthalpy, discharge pipe area, and lip pressure as follows (Grant and Bixley, 2011):

$$Q = 1,835,000A \frac{p_c^{0.96}}{H_t^{1.102}} \quad (14)$$

where Q = Total mass flow rate (kg/s);
 A = The cross-sectional area of the lip pipe (m²);
 p_c = Critical pressure at the end of the lip pipe (bar-a);
 H_t = The enthalpy of the fluid (kJ/kg).

Since the well is being discharged into the atmosphere, the specific enthalpies of steam and water at atmospheric pressure should be used:

$$Q = W \frac{(H_S - H_W)}{(H_S - H_t)} \quad (15)$$

where W = Water flow (kg/s);
 H_S = Steam enthalpy at atmospheric pressure (kJ/kg);
 H_W = Water enthalpy at atmospheric pressure (kJ/kg).

Combining Equations 14 and 15, gives:

$$1,835,000A \frac{p_c^{0.96}}{H_t^{1.102}} = W \frac{(H_S - H_W)}{(H_S - H_t)} \quad (16)$$

The enthalpy H_t , is the only unknown variable in Equation 16 and after combining the total mass flow rate, water flow rate, and steam flow rate, flow enthalpy and electric power can be calculated. The water flow W is related to the total mass flow (Q) by Equation 17:

$$Q = \frac{W}{1 - X} \quad \text{and} \quad X = \frac{H_t - H_w}{H_S - H_w} \quad (17)$$

where X = Steam mass fraction;

Specific enthalpies of water and steam should be looked up in the steam tables at separation pressure conditions.

Bodvarsson and Witherspoon (1989) pointed out that repeating flow tests using different sizes of lip pressure pipes enables the acquisition of varying wellhead pressure (WHP) with corresponding mass flow rates. Well productivity as a function of wellhead pressure can be determined by coming up with the characteristic curve, which can be used in selecting the operating conditions for the turbines in the power plant.

5.2 MW-1 discharge data analysis

MW-1 was allowed to heat up for 22 days after drilling before discharging. However, it did not build up sufficient pressure to enable self-discharge. It was, therefore, pressured for several hours which allowed the temperatures in the water column to recover, initiating discharge when the valves were opened. The well was tested using 5 sizes of discharge pipes (202, 155, 130, 104 and 80 mm). Table 3 below shows a discharge output summary. At the time of writing this report, the well was still being tested.

TABLE 3: Summary of output conditions during discharge

Pipe diameter (mm)	WHP (bar-a)	Total mass flow (kg/s)	Water flow (kg/s)	Enthalpy (kJ/kg)	Steam flow at WHP (kg/s)
Set 1 (29/5/2011 – 11/7/2011)					
202	7.9	59.4	40	1155.3	14.5
155	8.3	54.6	37	1150.7	13.1
130	9.4	54.2	34.6	1234.5	15.3
104	11.9	48	31.7	1210.7	13
Set 2 (13/7/2011 – 24/8/2011)					
202	6.9	51.8	34	1195.6	13.6
155	7.4	46.7	32.5	1115.3	10.6
130	8.4	47.9	31.2	1198.8	12.6
104	10.7	44.9	29	1217.3	12.3
80	14.5	40.3	25.6	1241.6	11.5
Set 3 (25/8/2011 – 21/9/2011)					
202	6.3	45	29.1	1213.5	12.2
155	7.3	44.5	29	1208.8	12
130	8.5	45.2	29	1231.2	12.7
104	10.3	42.8	27.6	1213.9	11.6

With over two and half months discharge testing, using different size discharge pipes, the well output seemed to stabilize. Figure 13 presents the output conditions since the start of discharge. In the beginning of the test the well yielded about 60 kg/s of which 20 kg/s were steam, indicating a generating capacity of up to 10 MWe. There was, however, a decreasing trend in well output for the first two sets of discharge using 202, 155, 130, 104 and 80 mm discharge pipes, but the third set presents more stable conditions in the well. Additional future data might present this stabilization more clearly. Varying wellhead conditions after 80 days seemed to have little effect on the well output in terms of mass, water and steam flow, with the total flow on the order of 45 kg/s, out of which approximately 30 kg/s is water and 15 kg/s is steam. Steam at WHP after 80 days of testing was close to 12 kg/s, indicating more than 6 MWe well capacity. Enthalpy, though, showed a slight increasing trend during the first 2 months of flow test, rising from about 1150 to over 1200 kJ/kg, indicating that it was not fully heated up when the flow test started. An enthalpy value of around 1200 kJ/kg suggests a mean inflow temperature of 275°C which agrees with the temperature log in the well and the estimated formation temperature (Figure 5).

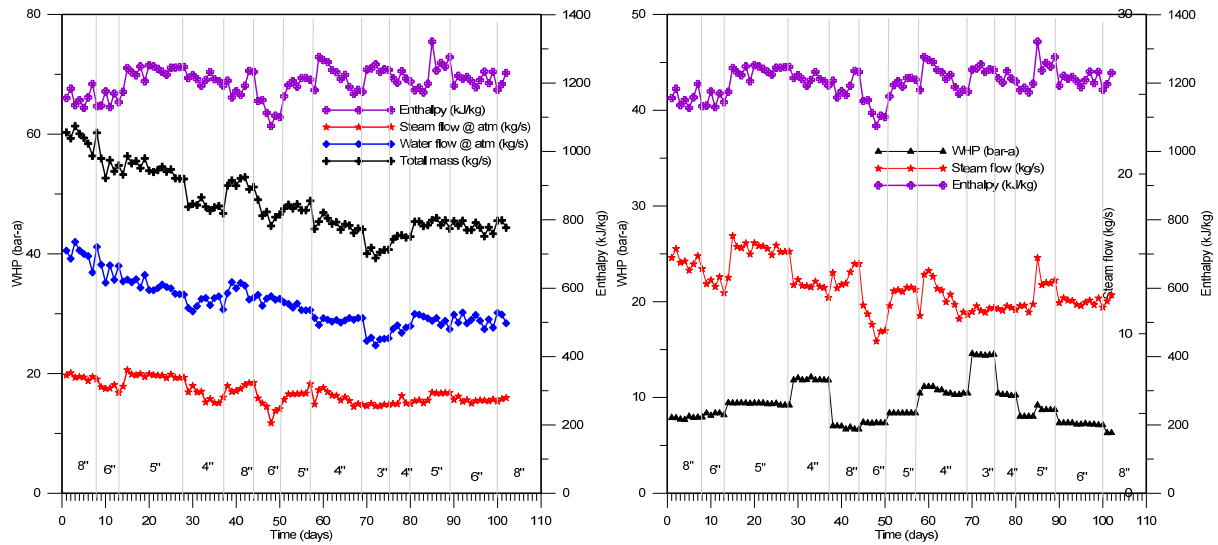


FIGURE 13: MW-1 discharge history with flow and enthalpy (left) and steam flow enthalpy and WHP (right)

The output curve relates the mass output with wellhead pressure. Figure 14 shows three output curves for MW-1 at different times during the flow test. The shut-in pressure has not been measured yet, but will be measured when the well is shut-in at the end of the discharge test.

6. GEOTHERMAL RESOURCE ASSESSMENT

6.1 Introduction

A geothermal resource can be defined as that fraction of the resource which is at depths shallow enough to be tapped by drilling in the foreseeable future, and that can be recovered as useful heat economically by using available technology (Williams et al., 2008). Muffler and Cataldi (1978) pointed to four methods for assessing geothermal resources, i.e. surface heat flux, volume method, planar fracture and magmatic heat budget. According to Williams (2007), the volumetric method has been widely established and has become the standard approach for assessing geothermal resources.

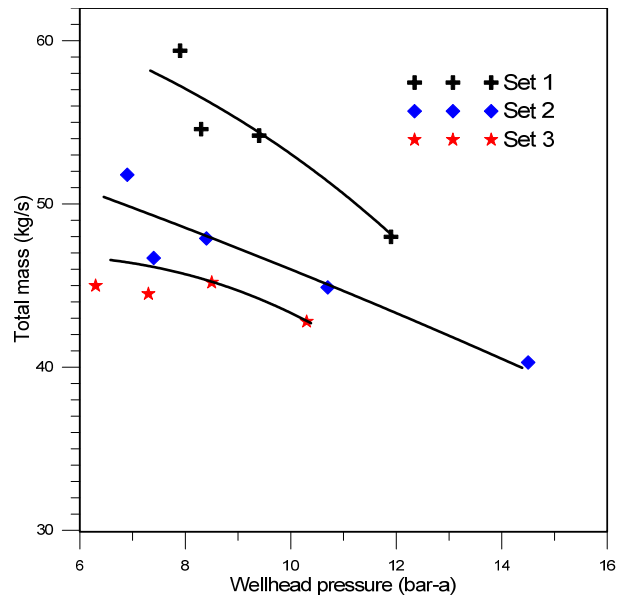


FIGURE 14: Output curves for MW-1 from three sets of discharge data (see Table 2)

In this report, an assessment of geothermal resources in the Menengai area was carried out to obtain the preliminary estimates of the reservoir within the caldera. The assessment was based on available information, which is rather limited. Future data will be used to update and refine the volumetric model.

The volumetric method is based on the calculation of the thermal energy in the rock and the fluid which could be extracted based on the specific reservoir volume, reservoir temperature and final or reference temperature (Sarmiento and Steingrímsson, 2011). Therefore, the total heat energy in a geothermal system is the sum of the heat energy from within the rock matrix and in the fluid. As

discussed by Halldórsdóttir et al. (2010), Equation 18 is used to calculate the heat contained in a geothermal system:

$$Q = \oint_v C [T - T_0] dV \quad (18)$$

where Q is the heat contained in the system, C is the heat capacity per unit volume, T is the reservoir temperature and T_0 is the reference (cut-off) temperature.

With the assumption that the heat capacity and temperature are homogenous in horizontal directions and that they vary only in the vertical direction, the heat content of a system can be calculated, using Equation 19 below, by integrating the heat capacity per unit volume $C(z)$ and the difference of the estimated temperature curve $T(z)$ in the system and the cut-off temperature T_0 .

$$Q = A \int_{z_0}^{z_1} C(z) [T(z) - T_0] dz \quad (19)$$

A is the surface area of the geothermal system.

In order to simplify, the geothermal system is often divided into different layers where the heat capacity is constant in each layer and depends only on the specific heat and density of the rock and water, respectively. Only a small portion of the stored heat in the reservoir can be extracted to the surface. This defines a recovery factor, R , (usually less than 25%) which can be used to calculate the recoverable heat Q_h in Equation 20:

$$Q_h = RAC \int_{z_0}^{z_1} [T(z) - T_0] dz \quad (20)$$

From the heat which is recovered from the geothermal system, a small portion can be converted into electric energy. Therefore Equation 21 is used to calculate the fraction of the heat that can be utilized for electrical power generation, where η_e is the conversion efficiency.

$$Q_e = \eta_e Q_h \quad (21)$$

6.2 Menengai caldera reserve estimation by Monte Carlo calculations

The Monte Carlo method used for reserve estimation within the Menengai caldera is a probabilistic method of the volumetric calculation which accounts for the uncertainty in many variables in geothermal reserve estimation (Sarmiento and Steingrímsson, 2011). Table 4 below shows the applied

TABLE 4: Parameters used in the Monte Carlo calculations for reserve estimation within the Menengai caldera

Parameter	Minimum	Best value	Maximum	Distribution type
Thickness (m)	2000	2500	3000	Triangular
Area	8	16	60	Triangular
Cut-off temperature (°C)	N/A	170	N/A	Fixed
Porosity (%)	5	N/A	10	Constant
Boil curve ratio (%)	50	80	100	Triangular
Recovery factor	10	20	25	Triangular
Convergence efficiency (%)	N/A	12	N/A	Fixed

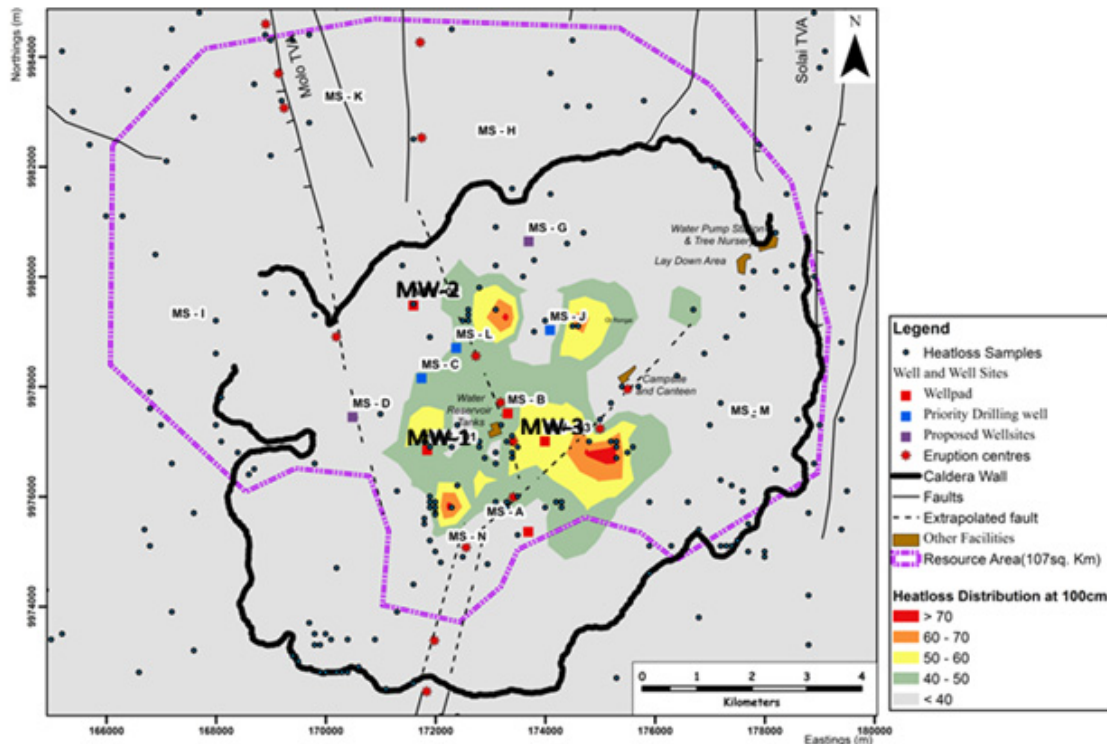


FIGURE 15: The Menengai geothermal field, showing the area with elevated temperature at the surface within the caldera (Lagat et al., 2010)

uncertainty distribution models used for the various input parameters for this analysis.

The total approximate area within the Menengai caldera (Figure 2) was used as the maximum size of the resource area. The maximum area was estimated to be approximately 77 km². The surface area, with indications of active surface activity, i.e. areas with more than 40°C, was used to obtain the most likely area (Figure 15). This gave approximately 19 km², while the minimum area was obtained by approximating the area occupied by exploratory wells, which is approximately 8 km².

In Menengai, the drilling programme is focussed around wells up to 3 km deep. Therefore, for the purpose of estimating the reserve within the caldera, the thicknesses are 2000, 2500 and 3000 m, the minimum, most likely and maximum, respectively. Currently, one well is 3000 m deep, while the other two are more than 2100 m.

Subsurface rocks obtained from well cuttings are mainly trachytic. The porosity of the rocks from this field has not been precisely determined. For comparison purposes, subsurface rocks in Iceland are mainly basaltic lavas and hyaloclastics with the porosity of the basaltic lavas ranging from 5 to 15% (Halldórsdóttir et al., 2010). Singhal and Gupta (2010) estimated the porosity of basaltic and trachytic rocks as ranging between 5 and 17%, depending on whether the rocks were fractured, weathered or vesicular. From this information, the porosity value for Menengai subsurface rocks, given that they are to some extent fractured, is assumed to range between 5 and 10%.

As discussed by Halldórsdóttir et al. (2010), when calculating the heat distribution throughout the reservoir, it is convenient for many geothermal areas to assume that a temperature curve follows a curve like that of the boiling point with depth. Equation 22 below describes a temperature curve shaped like the boiling point curve (James, 1970):

$$T(z) = X * 69.56((z - z_0)^{0.2085}) \quad (22)$$

where the X ratio factor describes the deviation from the true boiling point curve.

The X ratio ranges from 0 to 1, depending on how the formation temperature curves deviate from the true boiling depth (ratio 1). From the preliminary results from Menengai exploration wells, the formation temperatures are estimated to range from 0.5 to 1 of the boiling curve, with a most likely value of 0.8.

Muffler and Cataldi (1978) proposed a theoretical geothermal recovery factor as a function of reservoir porosity (Sarmiento and Steingrímsson, 2011; Pastor et al., 2010; Halldórsdóttir et al., 2010). Using the porosity values considered for this case, a recovery factor of 10% as minimum and 25% as maximum was used, with 20% as the best value.

Geothermal fluid from Menengai field will be utilized mainly for electricity generation. Geothermal fluid will also be utilised for direct uses in the nearby agricultural and industrial hub of Nakuru township. To obtain an estimate for the electric power that could be produced from the recoverable heat, 170°C was taken as the reference temperature (cut-off temperature).

Bodvarsson (1974) presented a relationship between reservoir temperature and conversion efficiency. Exploration well MW-1, having been flow tested, indicated an enthalpy of the fluid of around 1200 kJ/kg. This translates to a reservoir fluid temperature of around 275°C. Assuming the reservoir fluid in the area is in this range, the conversion efficiency value chosen is, therefore, 12%.

Using the above parameters, a random number generator in the Monte Carlo calculation solves the algorithm relating the uncertainty distribution. Several statistical parameters were calculated from the 10,000 random outcomes (generated from the Monte Carlo runs). The statistics calculated from the model are presented in Table 5. From Figure 16, it is most probable, with approximately 12% probability, that the electric power generating capacity from the area is approximately 1600 MWe for 30 years and 105 MWe for 50 years. Also, the statistics show that the volumetric model predicts with 90% confidence that power production capacity for 30 years within the Menengai caldera ranges between 40 and 570 MWe, and up to 375 MWe produced for 50 years. From Figure 17, the volumetric model predicts with 90% probability that at least 95 MWe

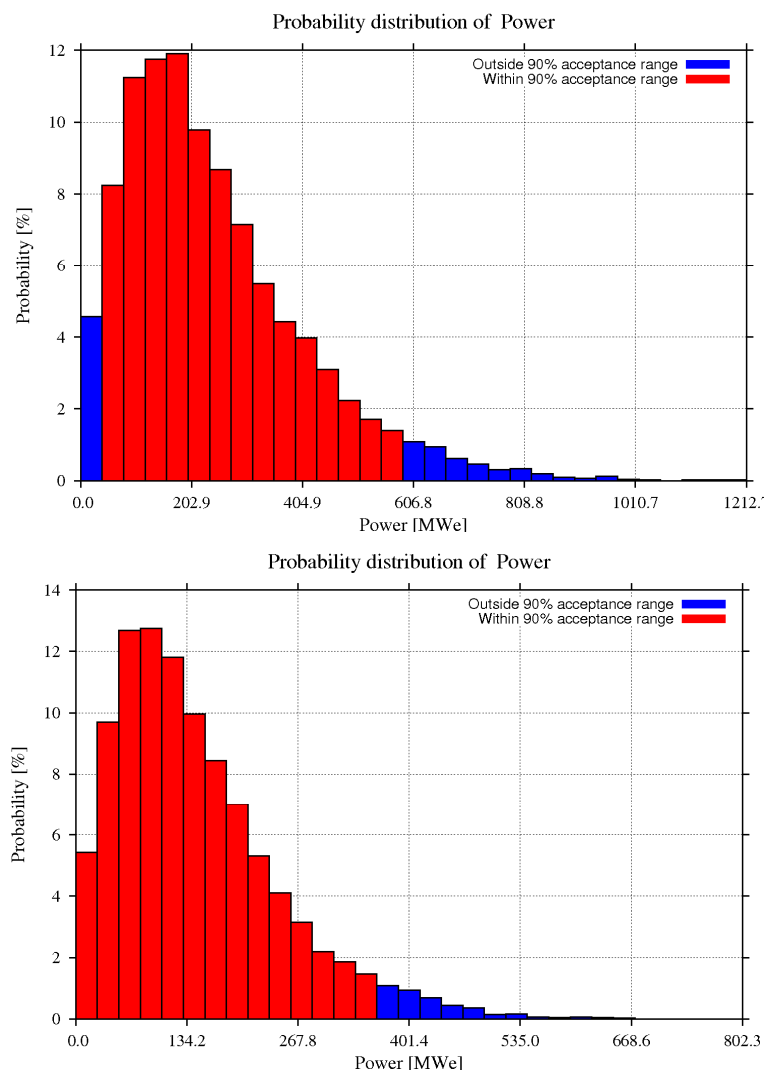


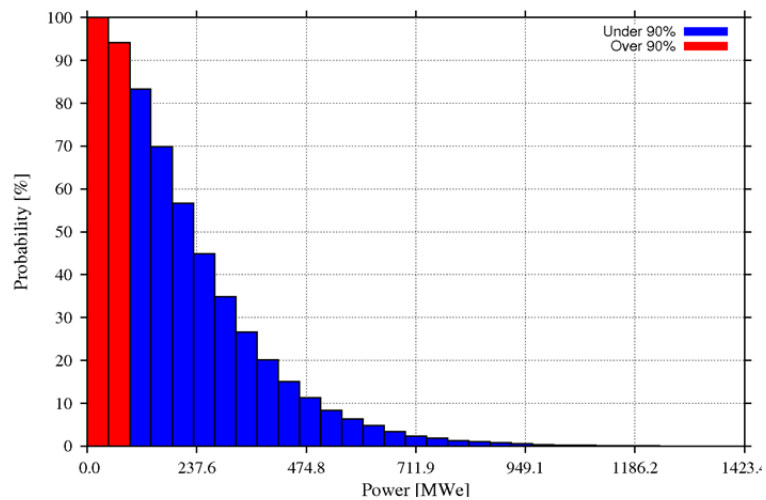
FIGURE 16: Probability distribution for electric power generation for 30 years (above) and 50 years (below)

TABLE 5: Statistical parameter estimates for the probability distribution for electric power production for the Menengai Caldera

Statistical sizes	Value (MWe)	Value (MWe)
	30 years	50 years
Most probable value	160	105
90% confidence range	40-570	Up to 375
Mean value	290	180
Median value	240	150
Standard deviation	210	130
90% limit	95	50

It is worth remembering that the parameters used in this volumetric model are approximate values from available data and appropriate assumptions on other parameters.

The wide range between the values generated can be attributed to the wide variation between the maximum and minimum areas. New data, as it becomes available, should be used to update this model.



7. DISCUSSION AND CONCLUSIONS

A preliminary analysis on well measurements and tests conducted in three exploration wells MW-1, MW-2 and MW-3 was made and the results presented. The three wells are still undergoing tests and measurements; therefore, the discussion is limited to available data.

- 1) Well MW-1 was drilled to 2195 m in the period from 12th February to 1st May 2011. The well was allowed to heat-up immediately after drilling for a maximum of 22 days, after which it was discharge tested. The main feed zones are at around 1050, 1800 and 2050 m depth. The pivot point was measured at 1500 m. The estimated formation temperature, 208°C at 900 m, suggests a conductive profile from the surface down to around 900 m depth, then a more or less convective profile to the well bottom, taking a shape similar to that of a boiling point with depth curve, although cooler. The bottom temperature is estimated at 298°C. The flowing temperature and pressure profiles indicate two-phase boiling fluid from the well bottom and probable boiling in the formation. Gassy inflow into the well causes a shift in the boiling point of the fluid.

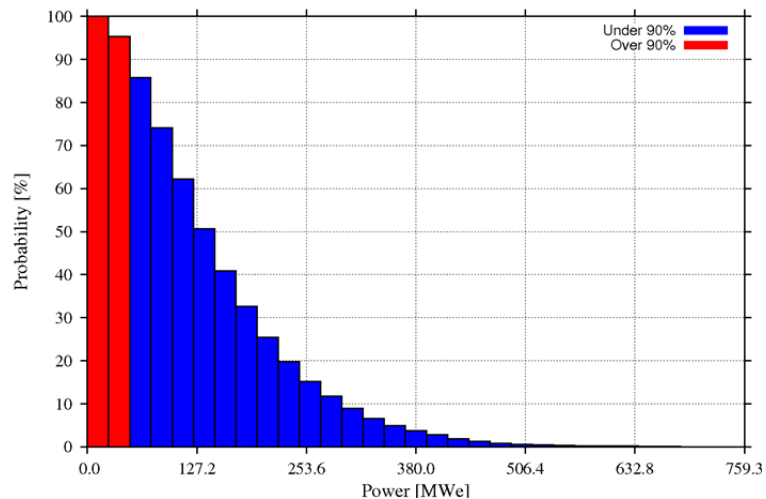


FIGURE 17: Cumulative probability distribution for electric power generation for a period of 30 years (above) and 50 years (below)

- 2) The discharge test conducted in MW-1 indicated fluid with an enthalpy of over 1200 kJ/kg, corresponding to fluid of around 275°C, which agrees with the flowing temperature logs. Initial flow from the well was of the order of 60 kg/s thereof 20 kg/s of steam. The well decreased in power during the 80 days which was attributed to incomplete heat-up conditions in the well prior to discharge. Stabilized discharge seemed to be attained after about 3 months, with a 130 mm discharge pipe giving the highest total output of around 45 kg/s, of which 12 kg/s is steam at over 8 bar-a WHP, translating to more than 6 MWe capacity.
- 3) MW-2 was drilled to 3189 m in the period from 28th February to 2nd July 2011. An injection test was conducted immediately after drilling. Injection of cold water into the well for a duration of 13 hours at varying rates resulted in pressure build-up of 7 bars. The well Injectivity Index (II) is on the order of 4 l/s/bar and storativity and transmissivity values are in the range 1.48×10^{-7} - 1.58×10^{-7} m/Pa and 8.56×10^{-8} - 11.7×10^{-8} m³/Pa.s, respectively. These are comparable to wells in the Olkaria geothermal field.
- 4) Temperature profiles during the heating-up period of MW-2 indicated the main feed zones are at around 1300, 2250 and 3000 m depth. The feed zone at around 1300 m, at only about 80°C, is responsible for cooling and masking temperature recovery all the way to the well bottom. The estimated formation temperature suggests a conductive profile from the surface down to near 800 m depth, followed by a temperature reversal down to around 2100 m, after which it becomes conductive with a temperature probably much higher than what is estimated in this report. MW-2 is cold and, thus, not a producer; however, considering the inferred transmissivity and well injectivity from the injection test, the well might be utilized in the future for re-injection.
- 5) MW-3 was drilled to 2101.5 m in the period from 1st June 2011 to 27th August 2011. It was allowed to heat-up immediately after drilling. Heat-up profiles for a maximum of 22 days presented a cold section between 1250 and 1550 m. Effects of the drilling might have greatly cooled this section which is thought to be the most permeable layer intercepted by the well. Attempts to compress the well might have further cooled this section, which had otherwise heated up as seen on the 19.09.2011 profile (8 days heat-up), resulting in a temperature reversal recorded after 14 and 22 days of heating-up. Future profiles will hopefully show the true state of the temperatures at this section. Furthermore, future heat-up pressure profiles should show the pivot point, which is expected to be somewhere around 1500 m. The section below 1600 m is conductive, with a possible minor feed zone at the bottom.
- 6) Generally, a permeable zone was observed between 1000 and 1600 m. This was the case in all three wells, MW-1, MW-2 and MW-3, and may be associated with a major permeability structure.
- 7) The preliminary volumetric calculations, using the Monte Carlo method, were carried out for the area within the Menengai caldera. By using a reference temperature of 170°C in the model, it is predicted with 90% probable confidence that power production within the caldera ranges between 40 and 570 MWe for a period of 30 years and up to 375 MWe for a period of 50 years.

ACKNOWLEDGEMENTS

I sincerely appreciate the opportunity granted me to undertake this course by Geothermal Development Company, through Mr Cornel O. Ofwona, manager of the Reservoir engineering department, and the United Nations University Geothermal Training Programme, through Director Dr. Ingvar B. Fridleifsson and Deputy Director Mr. Lúdvík S. Georgsson, for the award of the UNU Fellowship.

I am truly grateful to Mr. Benedikt S. Steingrímsson and Mr. Sigvaldi Thordarson for their tireless direct involvement in the supervision of this work. Their advice and assistance during the writing of this report imparted valuable knowledge to me. I am also appreciative to the following persons in their respective capacities: Mr. Páll Jónsson, Mrs. Saeunn Halldórsdóttir, Dr. Svanbjörg H. Haraldsdóttir, Mr. Ingimar G. Haraldsson, Ms. Thórhildur Ísberg, Mr. Markús A.G. Wilde and all the lecturers for different course units. Much thanks go to Mr. Joseph Wambua and to my colleagues who contributed in one way or another towards the completion of this report.

Finally, special thanks are for my family, Dan and Joy, for their support and for enduring my long stay in Iceland. I am grateful to God for his grace upon me and my family throughout my stay in Iceland.

REFERENCES

- Axelsson, G., 2011: *The physics of geothermal resources and their management during utilization*. UNU-GTP, Iceland, unpublished lecture notes, 76 pp.
- Bodvarsson, G., 1974: Geothermal resource energetics. *Geothermics*, 3, 83-92.
- Bodvarsson, G.S., and Witherspoon, P.A., 1989: Geothermal reservoir engineering part I. *Geotherm. Sci. & Tech*, 2-1, 1-68.
- Dunkley, P.N., Smith, M., Allen, D.J. and Darling, W.G., 1993: *The geothermal activity and geology of the northern sector of the Kenya Rift Valley*. British Geological Survey Research Report SC/93/1.
- Earlougher, R.C., 1977: *Advances in well test analysis*. Soc. Petr. Eng., Monograph 5, 264 pp.
- Garg, S.K., and Pritchett, J.W., 1989: Cold water injection into single- and two-phase geothermal reservoirs. *Proceedings, of the 14th Workshop on Geothermal Reservoir Engineering, Stanford University, Stanford, Ca*, 189-196.
- Grant, M.A., 1979: *Interpretation of downhole measurements in geothermal wells*. DSIR, Wellington, New Zealand, report 8, AMD-88, 66 pp.
- Grant, M.A., and Bixley, P.F., 2011: *Geothermal reservoir engineering* (2nd ed.). Elsevier Inc., 349 pp.
- Grant, M.A., Donaldson, I.G., and Bixley, P.F., 1982: *Geothermal reservoir engineering*. Academic Press, NY, 369 pp.
- Halldórsdóttir, S., Björnsson, H., Axelsson, G., Gudmundsson, A., and Mortensen, A.K., 2010: Temperature model and volumetric assessment of the Krafla geothermal field in N-Iceland. *Proceedings of the World Geothermal Congress 2010, Bali, Indonesia*, 10 pp.
- Helgason, P., 1993: Step by step guide to BERGHITI. User's guide. In: Arason, Th., Björnsson, G., Axelsson, G., Bjarnason, J.Ö., and Helgason, P., 2004: *ICEBOX – Geothermal reservoir engineering software for Windows, a user's manual*. ÍSOR – Iceland GeoSurvey, Reykjavík, report ISOR-2004/014, 80 pp.
- Horne, R.N., 1995: *Modern well test analysis, a computer aided approach* (2nd edition). Petroway Inc., USA, 257 pp.
- James R., 1970: Factors controlling borehole performance. *Geothermics, Sp. issue*, 2-2, 1502-1515.

Johnson, K., and Lopez, S., 2003: *The nuts and bolts of falloff testing*. Environmental Protection Agency, Region 6, 76 pp.

Jónsson, P., 2011: *Injection well testing*. UNU-GTP, Iceland, unpublished lecture notes.

Júlíusson, E., Grétarsson, G., and Jónsson, P., 2007: *WellTester.1.0b. User's guide*. ISOR – Iceland GeoSurvey, Reykjavík, report 2008/63, 26 pp.

Kuria, Z.N., and Woldai, T., 2003: *Groundwater exploration: A case study of the location of well field north of Nakuru town, Rift Valley Province, Kenya*. Report, 15 pp.

Lagat, J., Mbia, P., and Mutoria, C.L., 2010: *Menengai prospect: Investigations for its geothermal potential*. Contributions from: Njue, L., Mutonga, M., Malimo, S., Kanda, I., Kipngok, J., Mwakirani, R., Suwai, J., and Mutie, T. Geothermal Development Company - GDC, Kenya, Geothermal Resource Assessment Project, 57 pp.

Leat, P.T., 1985: Discussion on the geological evolution of the trachytic caldera volcano Menengai, Kenya Rift Valley. *J. Geol. Soc.*, 711-712.

McCall, G.J.R., 1957: *Geology and groundwater conditions in the Nakuru area*. Ministry of Works, Hydraulic Branch, Nairobi, technical report 3.

McCall, G.J.R., 1967: *Geology of Nakuru-Thompson Falls — Lake Rannington area*. Geological Survey of Kenya, report 78, 122 pp.

Muffler, P., and Cataldi, R., 1978: Methods for regional assessment of geothermal resources. *Geothermics*, 7, 53-89.

Mungania, J., 2004: *Geological studies of Menengai geothermal prospect*. KenGen Ltd., internal report, 18 pp.

Mwawongo, G.M., 2005: Kenya's geothermal prospects outside Olkaria: Status of exploration and development. Lecture 4 in: Mwangi, M.N. (lecturer), *Lectures on geothermal in Kenya and Africa*. UNU-GTP, Iceland, Report 4, 41-50.

Omenda, P.A. (editor), 2000: *Ranking of the geothermal prospects in the Kenya Rift Valley*. Contributions from: Lagat, J., Mungania, J., Mariita, N., Onacha, S., Simiyu, S., Opondo, K., Kubo, B.P., Ouma, P., Wetangula, G., and Kollikho, P., KenGen – Kenya Electricity Generating Company, Kenya, internal report, 121 pp.

Omondi, C., 2011: Borehole geology and hydrothermal mineralisation of wells MW-01 and MW-02, Menengai geothermal field, Central Kenya Rift Valley. Report 30 in: *Geothermal training in Iceland 2011*. UNU-GTP, Iceland, 737-773.

Pastor, M.S., Fronda, A.D., Lazaro, V.S., and Velasquez, N.B., 2010: Resource assessment of Philippine geothermal areas. *Proceedings of World Geothermal Congress 2010, Bali, Indonesia*, 5 pp.

Renner, J.L., Shook, G.M., Garg, S., Finger, J.T., Kasameyer, P.W., Bloomfield, K.K., Hirtz, P.N., and Mines, G.L., 2007: Geothermal engineering. In: Lake, L.W. (editor-in-chief), *Petroleum engineering handbook*. Society of Petroleum Engineers, 629 pp.

Roux, B., Sanyal, S.K., and Brown, S., 1979: Static reservoir temperature from temperature build up data. *Proceedings of the 5th Workshop on Geothermal Reservoir Engineering, Stanford University, Stanford, Ca*, 343-354.

- Sarmiento, Z.F., and Steingrímsson, B., 2011: Resource assessment I: Introduction and volumetric assessment. Presented at "Short Course on Geothermal Drilling, Resource Development and Power Plants", Santa Tecla, El Salvador, UNU-GTP and LaGeo, CD UNU-GTP SC-12, 11 pp.
- Simiyu, S.M., and Keller, G.R., 1997: Integrated geophysical analysis of the East African Plateau from gravity anomalies and recent seismic studies. *Tectonophysics*, 278, 291-314.
- Simiyu, S.M., and Keller, G.R., 2001: An integrated geophysical analysis of the upper crust of the southern Kenya Rift. *Geophys. J. Int.*, 147, 543-561.
- Singhal, B.B., and Gupta, R.P., 2010: *Applied hydrogeology of fractured rocks* (2nd edition). Kluwer Academic Publishers (Springer), 408 pp.
- Stefánsson, V., and Steingrímsson, B.S., 1990: *Geothermal logging I, an introduction to techniques and interpretation* (3rd edition). Orkustofnun, Reykjavík, report OS-80017/JHD-09, 117 pp.
- Strecker, M.R., Blisniuk, P., and Eisbacher, G., 1990: Rotation of extension direction in the Central Kenya Rift. *Geology*, 18, 299-302.
- Tiab, D., 1975: A new approach (pressure derivative) to detect and locate multiple reservoir boundaries by transient well pressure data. New Mexico Tech., MSc thesis, 137 pp.
- Wameyo, P.M., 2005: Magnetotelluric and Transient Electromagnetic Methods in geothermal prospecting, with examples from Menengai, Kenya. Report 21 in: *Geothermal training in Iceland 2005*. UNU-GTP, Iceland, 409-439.
- Williams, C.F., 2007: Updated methods for estimating recovery factors for geothermal resources. *Proceedings of the 32nd Workshop on Geothermal Reservoir Engineering, Stanford University, Stanford, Ca*, 24 pp.
- Williams, C.F., Reed, M.J. and Mariner, R.H., 2008: *Review of methods applied by the US Geological Survey in the assessment of identified geothermal resources*. Department of the Interior, US Geological Survey, 27 pp.